# USC Rocket Propulsion Laboratory: Experiences Modeling a Composite Combustion Chamber

Michael T. Kezirian[1], Steven A. Leverette[2], and Stuart L. Phoenix[3]

[1] *The Boeing Company, Houston, TX 77059 USA*

[1] *University of Southern California, Los Angeles, CA 90089 USA*

[3] *Cornell University, Ithaca, NY, 14850, USA*

***Abstract**: The University of Southern California Rocket Propulsion Laboratory (USCRPL) is developing a single stage sounding rocket that is intended to deliver a small electronics payload past the Kármán line at 100 km altitude. A full scale static firing of the solid fuel booster was required in order to obtain the necessary launch permits from the Federal Aviation Administration and Bureau of Land Management. Though successfully demonstrated in sub-scale static and flight testing, this entirely carbon composite combustion chamber experienced catastrophic failure during consecutive static firings. As part of the anomaly investigation into this ground test failure, the Composite Modeler for Abaqus/CAE was used to identify the root cause. The comprehensive model of the ground test was used to show that the ground failures were the direct result of loads applied by the thrust stand retention methods and a buckling failure of the thrust stand itself in the case of the second live-firing. In other words, the failure was a consequence of the ground test configuration. The capability and fidelity of the modeler enabled the simulation to account for motor pressure loads, along with the coupled bending, torsional, and compressive aerodynamic loads expected from the design flight profile. The observed failure mode was not relevant to the flight hardware for the flight conditions. These analytical techniques were used to support the decision to maintain the current design of the flight motor-case. This design was used to move forward with the development of flight hardware and the seeking of flight opportunities.*

***Keywords**: Wound Composite Modeler, Residual Stress, Fiber Composite Structure, Polymer*

## 1. Introduction

Attempts to fly small rockets to very high altitudes require relatively high performance characteristics. Since the total impulse of a vehicle of a particular scale is ultimately limited by the chemical performance of the selected propellant, a high mass fraction of propellant is required to achieve overall desired performance. The consequence of this is that any attempt to fly a vehicle on the order of an 8 inch diameter to over 100km will need to be highly weight optimized and will support very little payload, even with the highest performing solid propellants. One way to improve overall mass fraction is through staging. However, in the interest of reducing complexity associated with staging, and improve chances of a successful flight with limited development and testing budget, it is desirable that a single stage vehicle be used. It is possible to deliver a small payload (on the order of 10 lb) to this altitude using a single stage vehicle of this scale together with careful allocation of weight within vehicle structures.

A sounding rocket design has been developed that uses advanced composite materials to achieve a very high propellant mass ratio. The vehicle consists of a monolithic carbon fiber/epoxy composite cylindrical tube. The structure, rendered in Figure 1, which acts both as the airframe and vehicle skin, is internally subdivided using pressure-carrying aluminum bulkheads. This creates a combustion chamber for the solid propellant rocket motor. To further reduce weight, the airframe and thrust chamber are consolidated into a single structure, which carries both the aerodynamic loads and internal pressure loads. Additionally, the use of anisotropic composite materials allows the design of a laminated material with tailored strength in each of its principal directions. Eliminating any material that contributes strength in directions that do not require it means further weight savings can be realized.

For this University of Southern California Rocket Propulsion Laboratory (USCRPL) vehicle, preliminary sizing of these structures was performed using basic netting analysis. In this process, it was assumed that all structural loads are carried singularly by filaments loaded axially, and properties of the matrix were neglected for loads not in the fiber direction. For this analysis, all bending and off-axis loading of the fibers was neglected to achieve an approximate structural sizing. Consequently, significant factors of safety were incorporated into the design process to compensate for these approximations. These methods were successful in developing a number of hardware iterations which performed adequately in hydrostatic, hot fire and sub-scale flight testing. However, several failures were observed very late in the development and testing process for the flight qualification of this vehicle. These events led to the development of a more rigorous analysis capability within the design team for these types of structures, and a detailed investigation of these failures is being conducted with the intent of demonstrating that this aspect of the vehicle's current design is flight-worthy. Additionally, the motor-case structure was modified to have a somewhat higher factor of safety. This report deals primarily with the development of Finite Element Models and testing performed in support of this failure analysis and qualification.

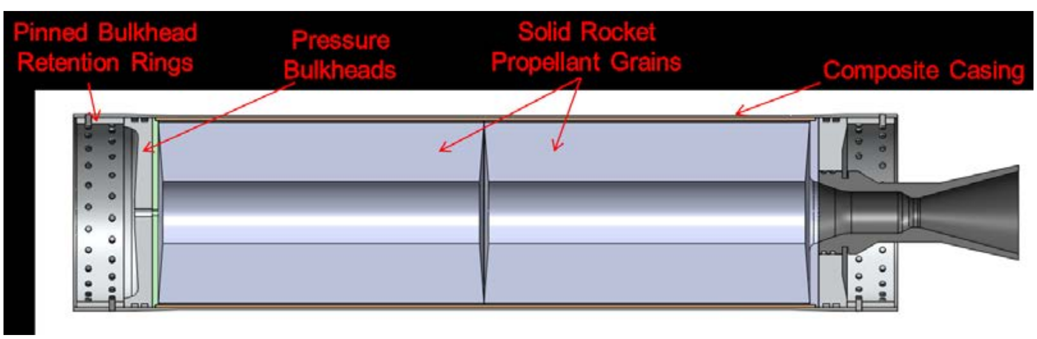


**Figure 1. “Minimum diameter" motor case design.**

## 2. Composite Design and Construction Methods

The primary structural element of the motor case being investigated is a monolithic carbon fiber-epoxy cylindrical tube. This composite part is created using hand-laid, unidirectional pre-impregnated, or pre-preg, material at orientations of 0, 45, and 90 degrees relative to the axis of revolution of the motor. As discussed earlier, the laminate layup schedule was determined using a basic netting analysis; the original part used in the static tests consisted of eleven (11) layers applied (or laid up) in this manner.

The updated layup schedule was intended to make the casing more robust, and prevent sensitivity to external loads for the flight vehicle. At the time it was assumed static failures were the direct result of test stand retention. It was recognized that increasing safety margin was desirable and would be accommodated if it were possible given the vehicle weight allocations. Total ply count for the unidirectional fiber was increased to fourteen (14) plies from eleven (11). Again, netting analysis was used to determine additional load capability. Relative to the original schedule, one extra 90 degree layer increased radial stiffness approximately 14% to decrease radial deflection. Two extra 45 degree plies provided about a 25% increase in axial stiffness, and an additional 12.5% increase in radial stiffness.

End closures were formed at either end of the motor using machined aluminum pressure bulkheads in contact with standard O-rings. Retention of these bulkheads is achieved using rings pinned through the composite by steel dowel pins. Bi-directional carbon weave is used to reinforce the pinned section of the composite part at both ends. Figure 1 shows all of these features on the 1/3 length test motor that will be discussed in the following sections. All features of this motor are common to the full-length flight motor, with the exception of the number of fuel grains, overall length of the motor, and throat dimension of the nozzle.

## 3. Previous Testing and Failures

### 3.1 Truncated Motor Testing

A hot-fire test of an 8 inch diameter carbon composite motor case was conducted in December, 2009. This motor was 1/3 the length of the space-shot motor and was intended to test the feasibility of an 8 inch diameter composite combustion chamber, the largest diameter composite case manufactured by USCRPL. The motor, shown in Figure 2, was retained in the thrust

**Figure 2. Truncated motor firing.**

stand by means of aluminum clamshell rings, which clamped the outside of the motor case. These restraints resist vertical and sideways motion, but allow a small degree of translational freedom along the thrust axis. Thrust data was collected directly using an S-type load cell. Chamber pressure measurements were recorded from a tap in the head end aluminum bulkhead using a pressure transducer.

During the first firing, the motor suffered a failure in the nozzle structure. This created a larger than nominal throat area and subsequent decrease in chamber pressure. An increase in burn time was also observed. However, the second live-fire test (Figure 2) of this motor took place in April, 2010 and was a complete success. The motor performed to nominal design predictions, reaching a pressure of around 800 psi and had a burn duration of approximately 10 seconds, proving the feasibility of the carbon motor-casing at this scale.

### 3.2 Flight Motor Testing

Following the successful firing of the truncated motor, construction began on a full length, 8 inch diameter motor, which was identical in construction to the truncated motor, with the exception of its increased length, the related increase in propellant mass and an updated nozzle geometry to maintain the nominal operating pressure. To assess the potential performance of the longer flight configuration, the full-length motor was tested on the same thrust stand as used previously.

**Figure 3. Frame-by-frame lead-up to motor separation.**

When ignited, the motor burned for around 1.5 seconds at which time the containment vessel separated radially, near the forward end. The combustion time was long enough for the motor to achieve a steady state operating pressure and for any startup transient effects to subside.

Examination of video recordings of the test indicated that failure was initiated immediately adjacent to the clamp rings retaining the motor in the stand. Figure 3 shows stills taken from this video, roughly 0.02 seconds apart. The first frame shows the motor in a steady state condition, immediately prior to the anomaly. The second frame shows the first traces of visible combustion gases escaping from the motor. The third and final frame shows not only a greater volume of escaping combustion gases, but also shows what appears to be a ruptured parcel of filaments deflected away from motor surface. The fiber rupture occurred along the forward edge of the retention clamp. A full rupture of the case immediately followed this image. The ensuing frame (not shown) is completely saturated with combustion products and no portions of the motor case or test stand remain visible.

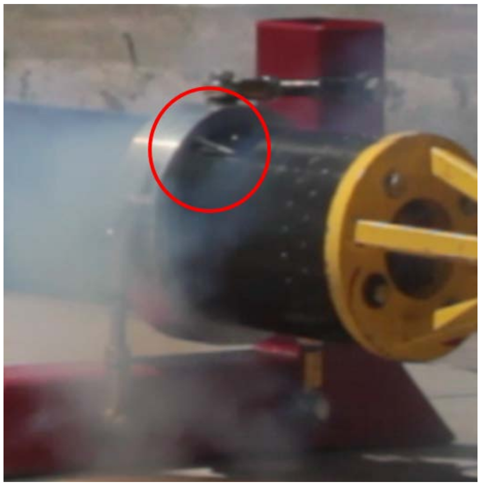

**Figure 4. Fiber separation visible prior to catastrophic failure.**

## 4. Finite Element Analysis of Composite Structures

In order to understand the failure observed during static testing, and to have improved confidence in the flight design, it was necessary to introduce more detailed computational methods for analyzing the USCRPL composite structures. Dassault Systemes Simulia's (DSS) Abaqus Complete Analysis Environment (CAE) 6.11-1 was used to develop a computational model and post-process the results generated from Abaqus Standard, Simulia's finite element solver.

**Figure 5. Flight motor static test: separated forward end of motor casing, fragment collected near test stand.**

**Figure 6. Flight motor static test: separated aft end of motor-case, fragment collected approximately 150 feet from test stand.**

### 4.1 FEA Methods

Approaching the analysis of this structure through finite element methods allows a detailed projection of the fiber loads, including cross-fiber shear and inter-laminar shear in addition to principal fiber loading. Simulia's Abaqus CAE was used to build up a finite element model - including all of the varying directional properties - of the composite casing. Using this software package, the fiber stress distribution can be determined in a deformed state, allowing insight not available to even the most detailed hand analyses. The application of the following analytical techniques, when used in conjunction with other diagnostic methods, are used to assess the operational worthiness of the USCRPL carbon composite motor case.

A 3-Dimensional continuum model of the rocket motor-case structure was developed in order to capture out-of-plane deformation of the structure. The solid brick elements used to create this model are assigned directional properties to reflect the anisotropic lamina behavior. In order to reduce the size of the FEA model and complexity of data extraction, the approach used was to build up an extremely thin revolved “sliver" of the pressure vessel laminate, including hardware fixtures such as the bulkhead retention rings and clamp rings. This “sliver" of the revolved body was then subjected to loads and symmetry constraints such that it replicated operating conditions of the pressurized part. Each ply of carbon tape, including the reinforcement stack-up at the ends, was modeled and assigned directional properties.

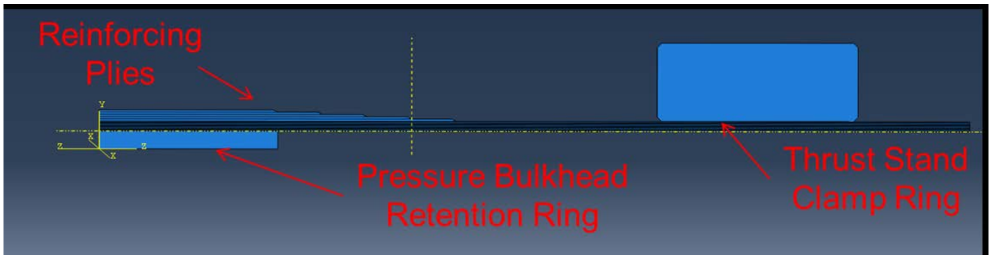


**Figure 7. Un-meshed finite element model components.**

A three-fold approach was taken to reduce analysis requirements:

1. Reduce quality of mesh wherever possible - reducing the mesh quality for low deflection parts like the aluminum rings will result in relatively little loss in the fidelity of results, but a significant reduction in computational time and resources.
2. Reduce non essential dimensions of model, such as sliver thickness - eliminating thickness reduces the amount of unnecessary “bulk" data being processed. Ideally this would be solved by using 2D shell elements in an axisymmetric model. Out of plane material properties necessitate utilizing a 3D model.
3. Truncate model wherever possible by using constraints and boundary conditions to replace regions of symmetry.

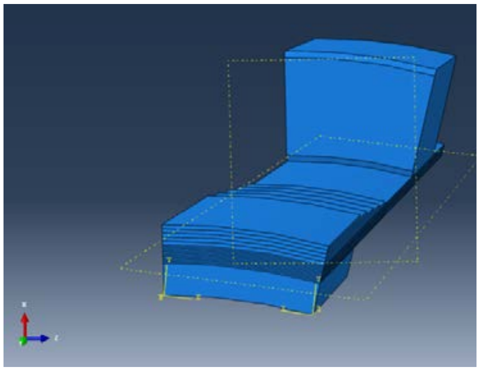

**Figure 8. Exaggerated part sliver.**

Targeting regions of symmetry allows large portions of the model to be cut out entirely with the right constraints - element count that previously went towards what may be considered "implicit" geometry can now go towards increasing mesh refinement throughout the composite part. Visual inspection of the strain /deflection contour results indicates that the middle portion of the pressure vessel is probably uniform in both stress and deflection. If it can be shown that this is true, the entire nozzle end, including the bulk of the mid-section, of the pressure vessel can reasonably be eliminated from the model using the appropriate constraints.

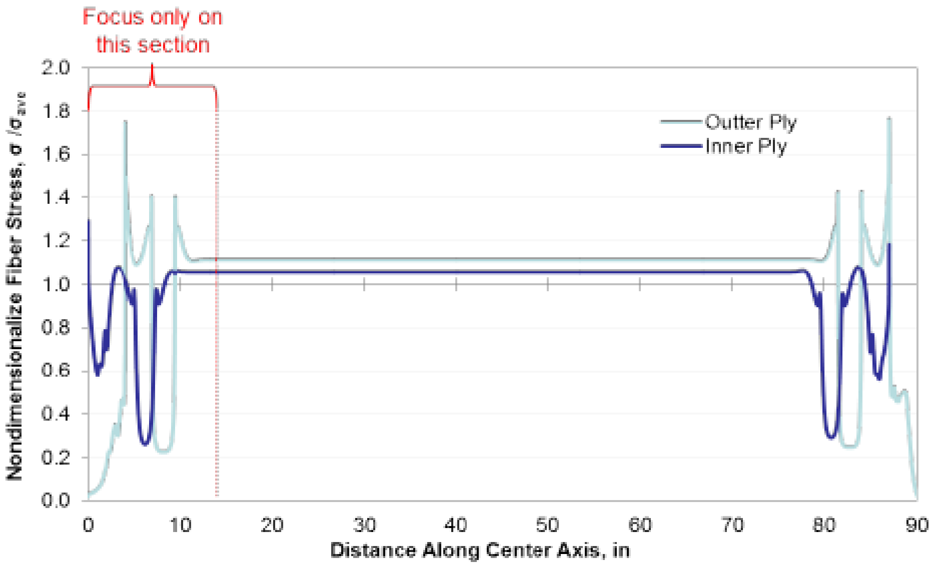


**Figure 9. Localized inner and outer ply stresses**

The stress plots of the principal fiber stress along the inner and outer plies (zero degree orientation) shows distinct similarity. Thus, it is possible to focus on a smaller but more densely meshed section of the geometry, replacing part of the model with anti-rotation or symmetry constraints, and remote loads. This method results in a memory overhead requirement of over 3x on a first pass.

## 4.2 Computational Results

### 4.2.1 Principal Fiber Stresses

Starting with the stress contour plots, problem areas can be identified. These contour plots are used to identify areas of interest as opposed to looking for actual stress values. These deformed plots provide valuable insight as to how the material is behaving and can offer clues as to what to look for in the numeric plots. The stress contour plots in Figures 10 and 11 show hot spots in the “shoulder” of fiber deflection near the clamp ring, and also identify a high stress area near the termination of reinforcing over-wrap layers.


Figure 10. Stress contour plot near overwrap terminations.

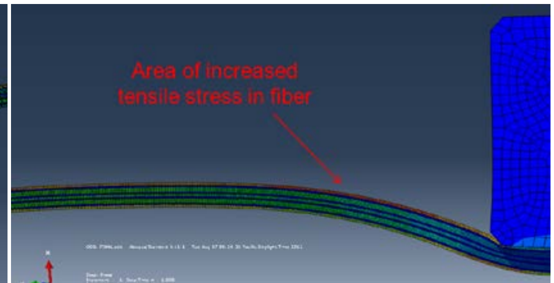


Figure 11. Stress contour plot in the overwrap near the clamp ring.

Figures 12 and 13 show how principal fiber stress in the axial plies is affected by the presence of clamp rings, starting from the forward end of the motor at X = 0. Local peaks in fiber stress are observed on either side of the retention clamp, at just past X = 6 inches and X = 8 inches. This plot indicates that the average stress in the fibers is decreased when the clamp is in place. This is because a portion of the hoop load is now carried by the retention ring. Stress concentrations in the axial fibers, however, are not indicated to be high enough to explain failure at this location. Note the stress at these concentrations is on the order of 1.0e5 psi, while the manufacturer indicated fiber rupture stress is on the order of 6.3e5 psi. A similar stress profile is observed in both axial carbon plies.

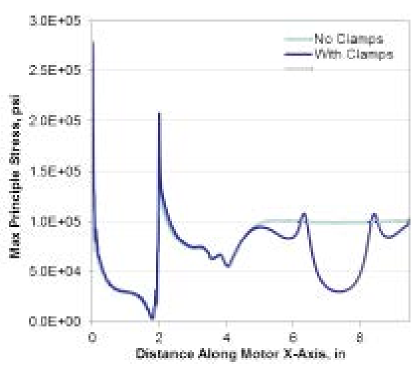


Figure 12. Principal stress 1 profile.

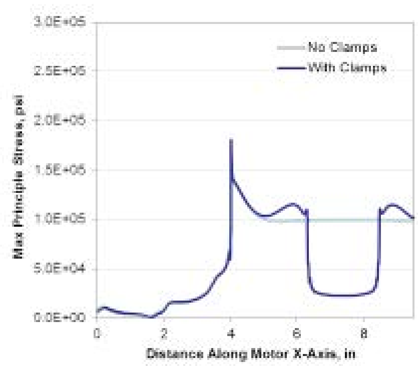


Figure 13. Principal stress 2 profile.

Concentrations in fiber stress also appear at the X = 2 inch location. These concentrations are related to the model construction and constraints, and it is believed that they do not necessarily reflect reality. A tied-surface constraint is used to bond the retention ring to the composite part in this model, whereas in reality, the composite part is pinned to the ring with dowel pins. Because these surfaces are not actually bonded, the sharp bending at the very corner of this ring will not be present. The transition that occurs here will be more gradual, and certainly more complex. This anomaly is a limitation of the computer model related to how detailed this component model is. This is a possible explanation for why failure was not observed here despite the fact that this is the highest indicated stress concentration in these plies.

If stress observed in the zero-degree orientation plies did not increase appreciably, it is possible that stress in the deformed condition was not re-distributed as anticipated. Figure 15 below shows principal fiber stress through the composite part thickness at a location adjacent to the clamp ring. Figure 14 shows the location of this cross-section stress plot, near the "shoulder" developed by the clamp constriction. The through-thickness stress, though slightly higher with the clamps, shows a profile similar to the un-clamped condition. This plot confirms that the highest loads are being carried by the zero-degree fibers on the inner and outer-most plies, and that the 45-degree plies are carrying somewhat less. Again, observed fiber stresses are well below the specified fiber strength so it is likely that something else has caused the failure.

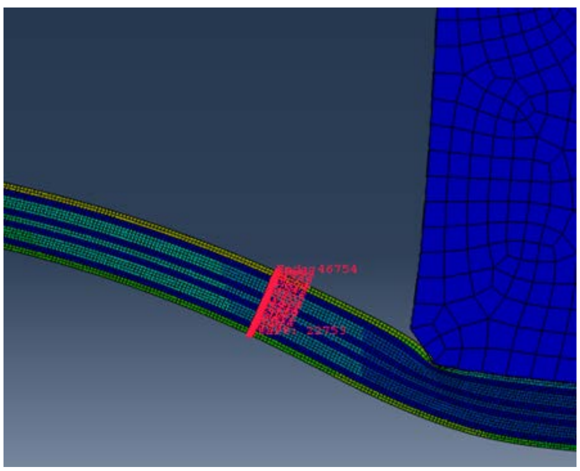

**Figure 14. Through-thickness path.**

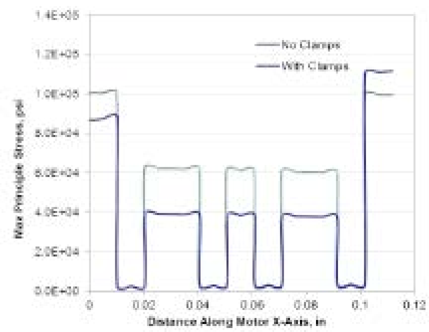


**Figure 15. Unclamped through thickness principal fiber stress.**

#### **4.2.2** Fiber Shear

Carbon filaments are very strong, and extremely stiff when loaded along the direction of the fiber, but can be very sensitive when loaded in shear, across the fiber axis. The same “pinching" effect of the clamp ring that cause the bending seen along the length of the part section necessarily imparts a significant shearing through the part thickness. Figures 16 and 17 show transverse shear in the axial plies along the motor axis of revolution, starting from the forward end. Comparing Figures 16 and 17 it is immediately clear that the presence of the clamp causes shear stress on the order of 1.0e4 psi in the outer-most ply. The effect on the interior axial ply is minimal, but present.

The unexpected results are the two high shear locations apparent in both the clamped and unclamped condition. The positive shear jump in the interior ply at around 2 inches from the front of the part correlates to the aft edge of the aluminum retention ring. This peak can be explained in a similar manner to the high tensile stresses predicted at this location - it is the result of a somewhat inaccurate constraint between the two bodies that creates an unrealistically "hard" transition point at the interface of these bodies. The result is a sudden change in perceived part thickness, and the overall apparent stiffness change creates a false reading of very concentrated shear at this location in the FEA model.

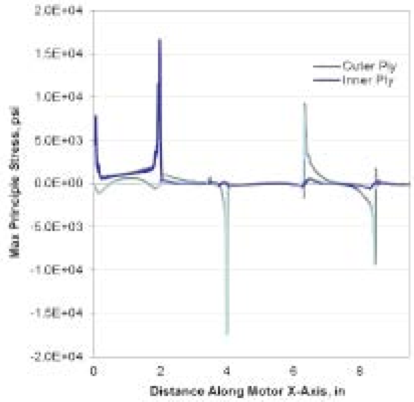


Figure 16. Shear stress in inner and outer plies with the clamp.

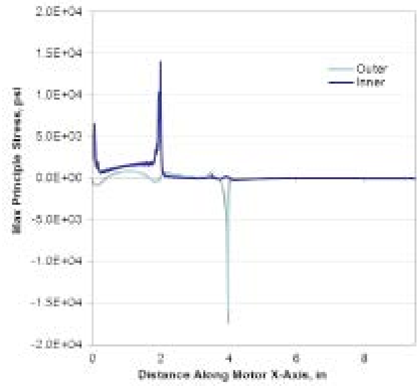


Figure 17. Shear stress in inner and outer plies without the clamp.

It is somewhat less intuitive why the significant negative jump in stress that is apparent in the outer ply has not caused failures in all phases of testing if the carbon fibers are sensitive enough in shear to fail under the loads caused by the clamp ring. The answer has to do with the stiffness of the bi-directional reinforcing plies at either end of the motor casing. The location of this phenomenon correlates to the termination of the last bi-directional overwrap, and the stiffness differential between the very last ply of overwrap and the unreinforced casing wall is significant enough here that instead of a gradual transition into the fully expanded state, there is a hard transition, causing high shear at this location. Effectively, the overwrap is causing a similar symptom as the clamp ring. The model suggests that this concentrated stress behavior ought to be as much of a failure driver as the clamp ring.  However, results observed in the testing portion of this project mitigate this concern somewhat, and will be discussed in the ensuing sections of this report.

### **4.2.3** Ply Elimination Study

In the shear stress study, high shear seemed to be localized toward the outer plies. In the interest of studying what redistributing effect a failure in the outer ply would have on the part’s ability to otherwise carry nominal loads, the outer-most fibers were “broken" and the principal fiber stress analysis repeated. This was done by assigning marginal material properties to a single element width of the outer ply. In this case, matrix properties were used as the marginal material properties.

Looking at the contour plot of principal stress in Figure 18, it is clear that maximum loading is now occurring on the inner ply near the outer edge of the retention ring, whereas before the “hot spot" in this area occurred on the outer ply. This demonstrates a capability to study the effect of fiber stress redistribution in the event of a local failure, and will be a valuable technique in continued failure analysis of this composite pressure vessel.

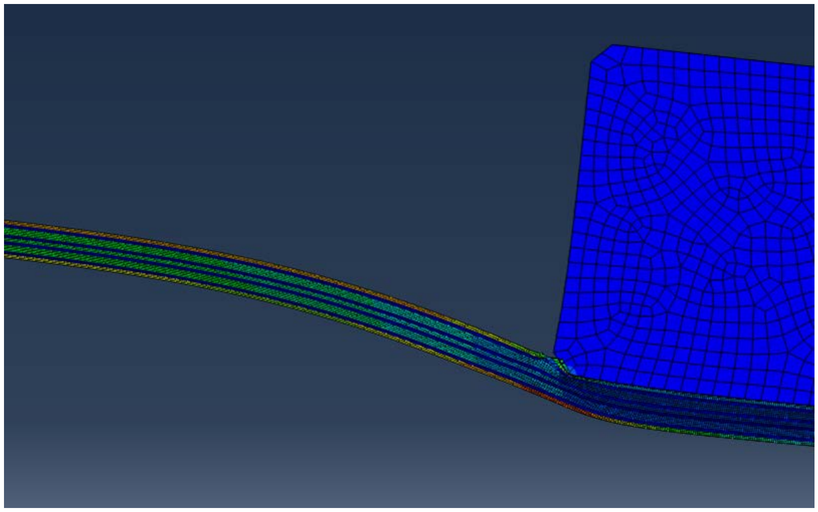

**Figure 18. Revised principal stress in the presence of a purposely failed ply.**

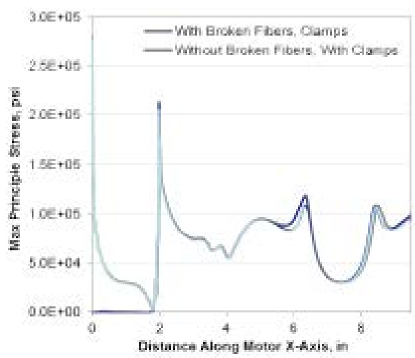


**Figure 19. Principal stress along motor axis near purposely failed ply.**

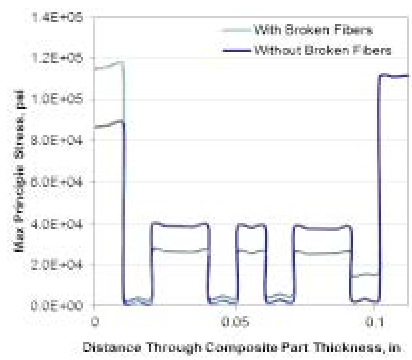


**Figure 20. Principal stress through the thickness near purposely failed ply.**

Figures 19 and 20 show stress distributions with and without fibers broken at the exterior surface. These plots indicate that with ruptured fibers, the stress redistribution is localized near the failure point. The effects do not seem to propagate very far axially. The through-thickness shift, however, is significant. It appears that more load is being carried locally by the interior ply, but the loading of the 45-degree plies is reduced.

#### **4.2.4** Computational Assessment of Updated Flight Design

The overarching objective of this study is to determine the flight-worthiness of the final composite motor-case to be used in the USCRPL sounding rocket. This is done primarily by proving that the failure mechanism in the test motor was caused by a thrust stand configuration and not a flaw in the design. However, despite the fact that the layup schedule has been updated slightly to be more robust, it is also prudent to demonstrate that the changes made do not introduce an additional unforeseen failure mechanism. Figures 21 and 22 compare principal fiber stress in the axial plies for both the old and new layup schedules.

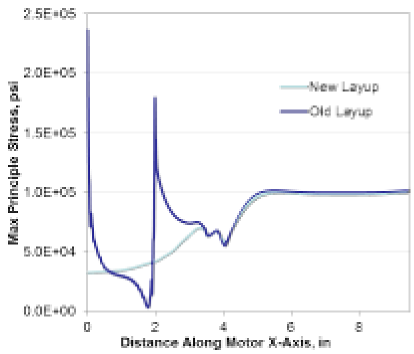


Figure 21. Comparison of principal stress 1 in new and old layup.

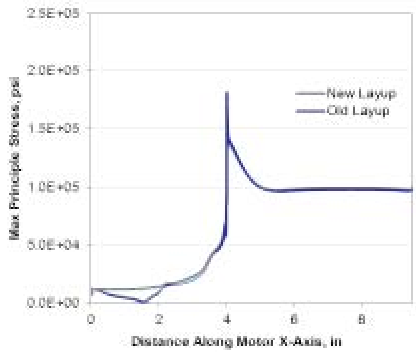


Figure 22. Comparison of principal stress 2 in new and old layup.

Slight decreases in principal stress are observed for the updated flight layup relative to the original. The slightness of the difference may be indicative of the fact that the bulk of the axial loading is still being carried by these two plies. Since they are the only two in this direction in either case, their loading may be similar. Regardless, the increased stiffness of the new part virtually eliminates the stress concentrations observed near the termination point of the reinforcing plies, further supporting the argument that this artifact is driven by the stiffness ratio between the overwrap and main structural plies. Ultimately, these figures do not indicate any more predisposition to failure than the prior casing.

## 5. Verification of FEA Results

Through several iterations on model specifications, it became clear that the results of the finite element analysis are highly sensitive to material properties. That is to say, not just the scale of the results, but also the shape of stress profiles and where the model indicates problematic areas can change greatly with what appears to be a minor alteration in the material inputs. This means that input parameters must reflect the as-built material properties. Ideally, finite element results must be validated against actual testing. The original 1/3 length motor case was used for comparative testing, as shown in Figure 23. The case has been instrumented in order to collect strain data.

This case was hydrostatically tested up to the mean operational pressure of 800 psi while collecting strain data at several key locations in both the hoop and axial directions. Particular attention was paid to collecting hoop stress data at several overwrap thicknesses as well over the un-reinforced composite part both near and far from the reinforcement termination point.

**(a)**

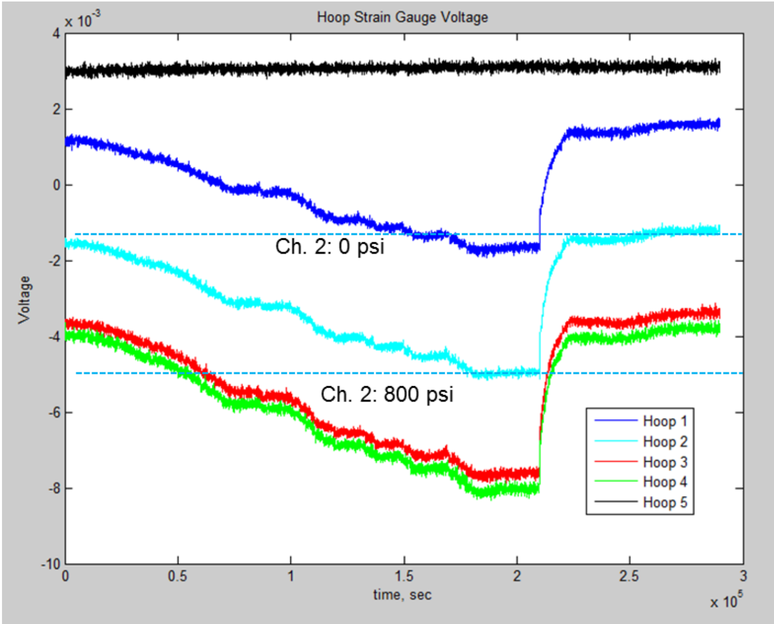


**(b)**

**Figure 23. Recorded strain gauge voltage over time at several locations (b) for hydrostatic testing at several locations (a). Steps for holds are visible in the time trace, and overall voltage differential is clearly visible. Strain values are recorded as time averaged data points at 0, 800 psi holds.**

The results of this test indicate that radial expansion over the reinforced sections was much greater than predicted by the finite element model. Radial expansion of the un-reinforced sections was much closer to expected values, and in some cases over-predicted strain in these locations. Sample strain values are given below in Table 1 for several data channels in the hoop direction during one test. Channels 1 and 2 are over reinforced sections, and Channels 3 and 4 are over unreinforced sections. What this data indicates is that either the anticipated stiffness of bi-directional reinforcements is significantly greater than reality, or the modeled ply thickness is larger than the as-laid up ply thickness of the reinforcement. The modeled ply thickness has been confirmed by measurements of the physical part, but as with the unidirectional fiber, no material property data has been collected for the bi-directional lamina. Because of this finding it is reasonable to question the validity of the shear stress concentration caused by the overwrap termination in the finite element model - at least until material property data has been collected for both fiber sets.

**Table 1. Original layup schedule for test motors.**

| Location | Measured | Finite Element | Percentage |
|---|---|---|---|
| 1 | 1.00e-3 | 2.40e-4 | 24.0% |
| 2 | 1.20e-3 | 7.63e-4 | 63.6% |
| 3 | 1.30e-3 | 1.27e-4 | 98.0% |
| 4 | 1.30e-3 | 1.55e-4 | 119.4% |

## 6. Conclusion

The University of Southern California Rocket Propulsion Laboratory is developing high-performance composite rocket motor-cases. This development process has led to increasingly more sophisticated analysis methods, recently culminating in diagnostic work performed on a motor case which failed during testing. A high-quality finite element model was generated and processed using Simulia's Abaqus CAE/standard which reflected all the orientation-specific material properties used in the construction of the composite structure. This analysis is currently being used to pinpoint the mechanisms which caused the motor failure, and support moving forward with an updated flight design. Preliminary results, as reinforced by strain measurement of existing test articles, indicate that the flight configuration of this motor is a viable design.

## 7. Acknowledgments

USCRPL is an undergraduate student research group in the Viterbi School of Engineering that is internally managed. The Authors thank The University of Southern California Department of Astronautical Engineering Chair and USCRPL Advisor Dr. Daniel Erwin, for his support of USCRPL and the ongoing research. They would also like to thank Simulia South Technical Expert, Mike Shubert, for technical support, and Dassault Systems research software licensing.